v. 4, n. 1, 2024

Journal of
Engineering
Research

MONTE CARLO STUDY ON UNCERTAINTY DUE TO POSITIONING IN A FULL BODY COUNTER

Ester Maria Rodrigues de Andrade
``Universidade Federal de Minas Gerais``` - UFMG
Belo Horizonte – MG
http://lattes.cnpq.br/5023025502934598

Daniel de Castro Pacheco
``Centro de Desenvolvimento da Tecnologia Nuclear`` - CDTN
Belo Horizonte – MG
http://lattes.cnpq.br/0207136434699068

Bruno Melo Mendes
``Centro de Desenvolvimento da Tecnologia Nuclear`` - CDTN
Belo Horizonte – MG
http://lattes.cnpq.br/7016638154017973

Abstract: The objective of this study was to evaluate the uncertainties due to the displacement of the occupationally exposed individual (IOE) in a full-body counter using the MCNP6 Monte Carlo code. The whole body counter (CCI) of an in-house dosimetry laboratory was modeled in MCNP6. The adult male ICRP reference phantom (RCP_AM) was positioned within the CCI at sixteen different positions along the longitudinal axis of the model at 5 cm intervals. The detection efficiency was evaluated at each position for monoenergetic photons of 100, 300, 500, 1,000, 1,500 and 2,500 keV. Two biodistribution configurations were simulated: source uniformly distributed in the soft tissues or lungs of the RCP_AM. In each case, the position with the highest efficiency was considered a reference for in vivo monitoring, and the error of the other positions in relation to the reference was calculated. Greater efficiency was found in the center of the abdomen in the lumbar spine region (P11) for soft tissue sources. Shifts of up to 10 cm from the RMP resulted in differences of less than 2.5% for all energies tested, except for 2500 keV, where the differences were less than 5%. In cases with a source in the lungs, IOE positioning errors were greater. Errors of less than 5% were observed only in the 5 cm band around the monitoring reference position, which was located over the sternum (P5), except for 100 keV photons, for which errors reached 6%. It was possible to conclude that errors due to displacement in the longitudinal axis will depend on biodistribution and must be greater when the activity is concentrated in a specific organ. Other biodistributions must be studied in the future, as well as errors arising from displacements of transverse axes.
Keywords: Internal Dosimetry; Incorporation; Full Body Counter; Monitoring uncertainties.

INTRODUCTION

Internal dosimetry makes it possible to calculate doses in occupationally exposed individuals (IOE), individuals in the general population and even in other living beings, due to the incorporation of radioactive materials (ICRP, 2015; Li, 2018; Paquet, 2022; Paquet et al., 2016).

An important step in calculating the compromised absorbed doses in the organs and the compromised effective dose is the determination of the activity incorporated by the individual through bioassays. Indirect (or in vitro) methods can be used to estimate incorporated activity. The vast majority of these methods consist of determining the activity excreted in urine or feces and the subsequent correlation between the amount excreted and the amount incorporated. Another alternative is to use direct methods (or in vivo counting). In these cases, detectors (usually scintillators or semiconductors) are positioned to quantify and qualify photon emissions originating directly from the human body or from specific organs such as the thyroid, liver and lungs (Breustedt, Giussani and Noßke, 2018; Desorgher et al., 2022; Paquet, 2022).

In vivo counting procedures, in general, are quick and convenient and have good accuracy for estimating the activity present in the body at the time of monitoring (ICRP, 2015). However, they can only be applied in cases of contamination by radionuclides that emit radiation that passes through the body and interacts with the detector, such as: gamma rays, X-rays and annihilation photons (Desorgher et al., 2022; ICRP, 2015).

The main uncertainties in in vivo measurements are associated with count statistics, Type A, and Type B uncertainties. The latter are mainly related to the anatomical variations in the shape and size of the human body, the variation in radioisotope biodistribution, the level of background, and

the positioning of the detector in relation to the body (Bouville, 2009; Breustedt, Giussani and Noßke, 2018; Desorgher et al., 2022).

Previous work has already evaluated several of these sources of uncertainty in in vivo monitoring systems (Bouville, 2009; Desorgher et al., 2022; Fonseca et al., 2014; Mendes et al., 2016; Zhang, Mille, and Xu, 2008). This work proposes to evaluate the uncertainties arising from the displacement of the longitudinal axis of the occupationally exposed individual (IOE) in a bed-type full-body counter installed in the Internal Dosimetry Laboratory of a Brazilian Nuclear Institute. As this type of CCI is commonly used for in vivo measurements, the results of this study may be useful to other laboratories.

MATERIALS AND METHODS

The Whole Body Counter (Figure 1A) of the CDTN Internal Dosimetry Laboratory was modeled on the MCNP6.1 code (Goorley et al., 2013). The simulated CCI geometry was developed and validated for local background simulations in previous work and can be seen in Figure 1B (Pacheco, 2023). In this study, the ICRP reference male phantom, RCP_AM, (ICRP, 2009) was simulated in the supine position inside the CCI and the counting efficiency was evaluated at 16 different points, in the longitudinal axis, spaced every 5 cm (Figure 1C).

The chemical composition and tissue density of RCP-AM were defined according to ICRP Publication 110 (ICRP, 2009). In the case of the CCI structures, including the lead shields and the 8"x4" NaI(Tl) detector, information on composition and density can be found in the work of Pacheco (2023) and in the Compendium of Material Composition Data for Radiation Transport Modeling (Pacheco, 2023; PNNL, 2021).

Two types of source distribution were modeled to emulate radioisotopes incorporated into the body: i) source uniformly distributed in the soft tissues of the RCP_AM; and ii) source uniformly distributed in the lungs. This choice of biodistributions reflects two contamination conditions commonly evaluated in in vivo systems. Positions P1 to P11 were evaluated for the source distributed in the lungs and positions P5 to P16 for the source distributed in soft tissues. Monoenergetic photons of 100 keV, 300 keV, 500 keV, 1000 keV, 1500 keV and 2500 keV were simulated in the two biodistribution configurations and for each of the defined positions. A total of 138 cases were executed. This way, it was possible to evaluate the counting efficiency as a function of energy for different positions of the phantom, considering the two proposed biodistributions.

Secondary particle transport was taken into account with Mode P E. The MCNP6.1 standard libraries for photon and electron transport were used (mcplib84 and el03, respectively). Likewise, the energy thresholds (cutoffs) for radiation transport used were also the code standards (1 keV) for photons and electrons.

The F08:p tally was used to evaluate the energy distribution of photon pulses occurring in the sensitive volume of the NaI(Tl) detector. The pulses were counted in 1,024 energy bands, incremented by 3 keV (e08 0 1e-5 0.003 1022i 3.072). This increase was used to emulate the configuration used in the NaI(TL) detector of the in vivo system used in practice, which has 1024 channels. The counting efficiency was calculated from the number of pulses counted in the channel corresponding to the energy of the photons simulated at the case source, per photon emitted at the source. For example for a 100 keV photon source, the number of pulses in bin #33 (99 keV to 102 KeV) per emitted photon was considered.

The number of stories of photons emitted

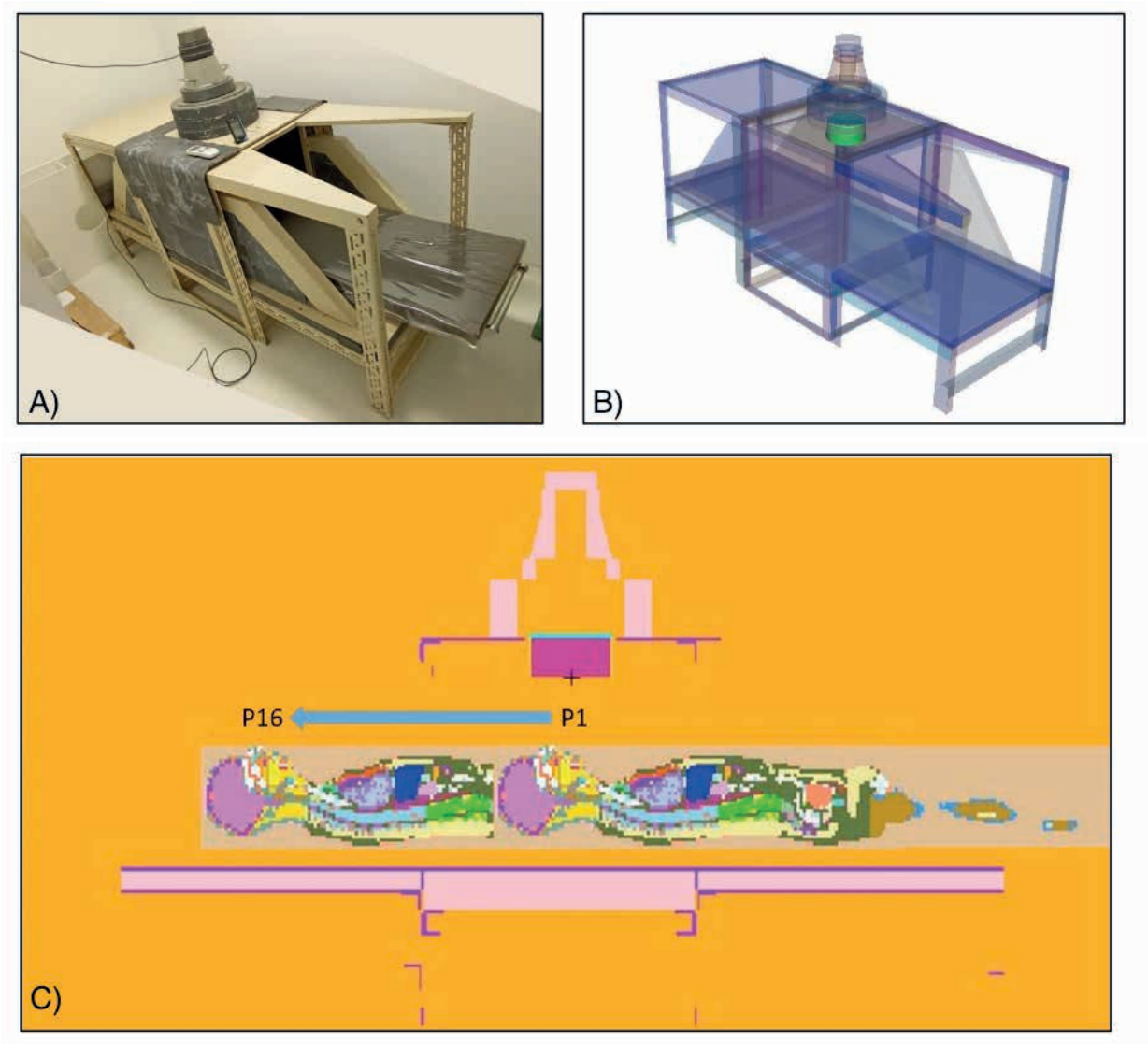

Figure 1: (A) LDI/CDTN whole body counter (CCI). (B) Image of the Vised® software showing the CCI simulation implemented in the MCNP6 Code. (C) Image adapted from the MCNP plot mode demonstrating the range of positions, in the longitudinal axis of the CCI, in which the RCP_AM phantom was simulated to evaluate the efficiency.

at the source that were followed (NPS) was 2.0E6 for cases with sources in the lungs and 1.0E7 for cases with the source distributed in soft tissues. Relative errors of less than 2% were expected for these NPS.

At the end of the simulations, the point of maximum efficiency for each biodistribution was considered the Reference Position for Monitoring (PRM = 0 cm) and the efficiency values as a function of energy at these points were plotted on graphs considering the two types of biodistribution. Graphs of efficiency versus PRM distance and error in relation to maximum efficiency points were plotted. The error in relation to the reference point for monitoring was calculated according to Equation 1, below:

$$Error = [(Ef_{Pi} - Ef_{PRM})/Ef_{PRM}] \cdot 100 \quad (1)$$

where, Ef_{Pi} is the efficiency at point Pi, which ranged from P_1 to P_{11} for the lung source and P5 to P16 for the soft tissue source; and EfPRM is the efficiency at the reference point for monitoring, PRM, obtained for each type of biodistribution.

The PRMs for each type of biodistribution were plotted on a representative figure of the in vivo system studied to help position the IOE in the future. From these points, error ranges smaller than 5% and 10% due to the positioning of the IOE, represented by the RCP_AM phantom in this study, were estimated and represented in the figures.

RESULTS AND DISCUSSIONS

LDI CCI simulations were run. The computational time (CT) of each simulation with the source in soft tissues ranged from 288 min to 1855 min, using only one processor core. In cases of source in the lung, the CT ranged from 105 min to 448 min. This difference was mainly due to the higher NPS used in cases with the source in soft tissues. The computational effort increased proportionally to the photon energy in both types of source distribution. Relative errors (RE) were less than 1.5% in all results. In soft tissue source simulations, the average ER was 0.6% and, for the lung source, 1.0% considering all points and all simulated energies.

The points at which the highest efficiencies were observed, considering the source distributed in the soft tissues and lungs, were P_{11} and P_5, respectively. In simulations with the source in soft tissues, the highest efficiency was 4.11E-03 pulses/photon observed for 300 keV photons, as shown in Figure 2A.

With the source distributed in the lung, the highest efficiency was 8.21E-03 pulses/photon, also for an energy of 300 keV (Figure 2B). Experimental and computational studies have demonstrated that the maximum counting efficiency for NaI(Tl), 8”x4” used in in vivo monitoring systems is observed in the range of 300 keV (Ferreira et al., 2023; Paiva et al., 2016 ; Santos, 2012). The counting efficiencies for the source distributed in the lungs were 1.8 to 2.0 times higher than the efficiencies obtained for the source distributed in the soft tissues for energies of 2500 keV and 300 keV respectively.

The efficiency curves as a function of distance from the PRM were obtained for the source distributed in the soft tissues (Figure 3A) and showed a flatter profile than the curves obtained for the source distributed in the lungs (Figure 3C). This fact was expected, since the source is concentrated in a smaller volume when distributed in the lungs.

Likewise, a steeper drop in efficiency is expected as the detector moves away from the point of highest efficiency, as seen in Figures 3A and 3C.

The flatter profile of the efficiency curves as a function of displacement in the longitudinal axis was reflected in a zone of 29 cm with positioning errors smaller than 5% and 45

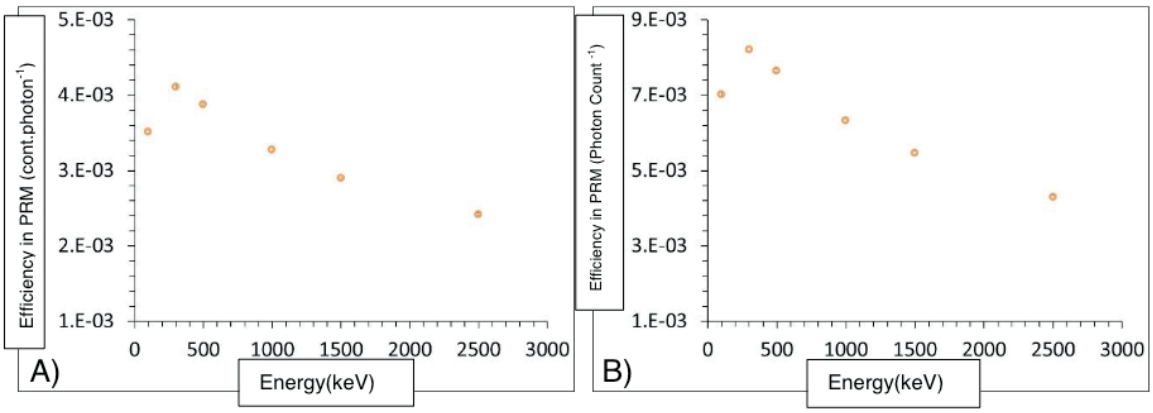

Figure 2: Maximum detection efficiency as a function of energy obtained for simulations of uniformly distributed sources in soft tissues (A) and lung (B). In the case of soft tissues, the maximum values were obtained at point P11. Point P5 showed greater efficiency considering the source in the lungs

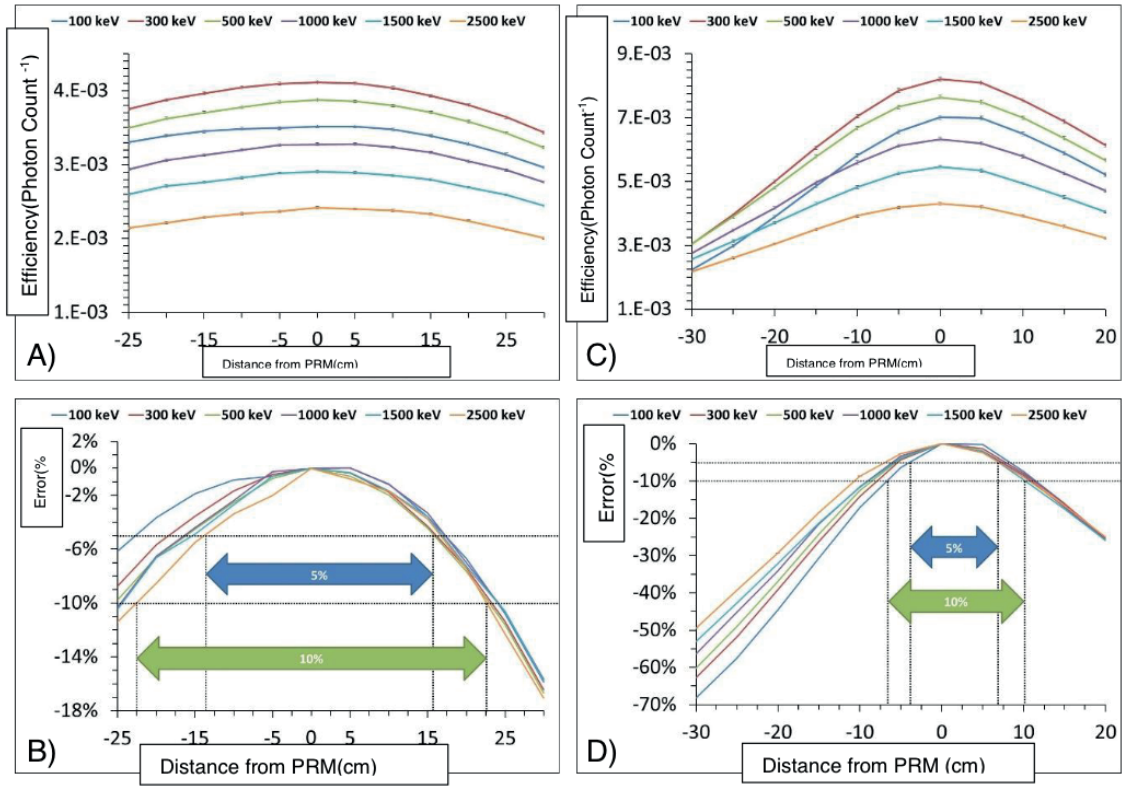

Figure 3: Detection efficiencies as a function of the position of the RCP_AM model within the CCI for various photon energies obtained in simulations of uniformly distributed sources in soft tissue (A) and lung (C). Graphs of efficiency differences as a function of distance from the estimated PRM for simulated sources in soft tissues (B) and lungs (D) were also included. The blue arrows indicate the area whose positioning errors in the longitudinal axis are less than 5% and the green arrows indicate the area with errors less than 10%.

cm with errors smaller than 10%, considering all photon energies evaluated and the source distributed in soft tissues (Figure 3B). Such zones were wider for 100 keV and 300 keV photons. It must also be noted that 10 cm shifts of the PRM resulted in differences of less than 2.5% for all tested energies of the female reference phantom, except for 2500 keV (3.4%).

In the case of the lung, however, the zones were much more restricted: 10 cm for errors smaller than 5%, and 16 cm for errors smaller than 10% (Figure 3D). Errors smaller than 5% were only found for distances smaller than 5 cm from the PRM. Unlike what was observed with sources distributed in soft tissues, for sources in the lung, the zones were wider for photons of higher energies such as 1500 keV and 2500 keV.

The locations of the points of highest counting efficiency (PR) can be seen in Figure 4. In cases of sources distributed in soft tissues, the abdomen/lumbar spine region (P11) presented the highest detection efficiency for photons of all ranges of energy evaluated, as can be seen in Figures 4A and 4B. In practical terms, for positioning the IOE at the time of monitoring, it can be established that the detector must be positioned in the abdominal cavity without its cranial end exceeding the rib region.

For sources distributed in the lung, point P5, located over the lungs (Figures 4C and 4D) showed greater efficiency. Based on the results of this work, it can be stated that a good landmark for positioning the detector on the IOE is the base of the neck. In this case, the cranial end of the detector must be positioned at the base of the neck.

In general, it was observed that the detection efficiency varied considerably for the two different biodistributions studied. This fact was evidenced in other works (Desorgher et al., 2022; Lamart et al., 2009; Mendes et al., 2019) demonstrating the importance of studying the influence of biokinetic parameters on detection efficiency and, fundamentally, on calculations of compromised effective dose.

CONCLUSÕES

Uncertainties due to positioning errors in the longitudinal axis of the occupationally exposed individual (IOE) in a bed-type whole-body counter were evaluated taking into account photons from 100 keV to 2500 keV and two biodistribution possibilities.

The most efficient positions were found for the detector positioned over the abdominal cavity for the soft tissue source and over the external bone for the lung source.

The efficiency of the system in PRM was 1.8 to 2.0 times greater for the source in the lung compared to the source distributed in all soft tissues. This fact emphasizes the need to adapt specific counting geometries when a high concentration of activity is found in a specific organ or tissue.

Differences in CCI efficiency were considered low when the source was established in soft tissue: displacements of 10 cm resulted in differences of less than 2.5%. The same cannot be said when the source is defined in the lungs. In these cases, errors greater than 3.0% must be expected for positioning errors of 5 cm or less.

The results of this study point to the importance of understanding and individualizing the biokinetic parameters of incorporated radionuclides, as well as knowing the specific efficiency of each in vivo counting system for different biodistributions. Other biodistributions for specific organs must be studied in the future, as well as errors arising from displacements of the transverse axis.

THANKS

The following Brazilian institutions

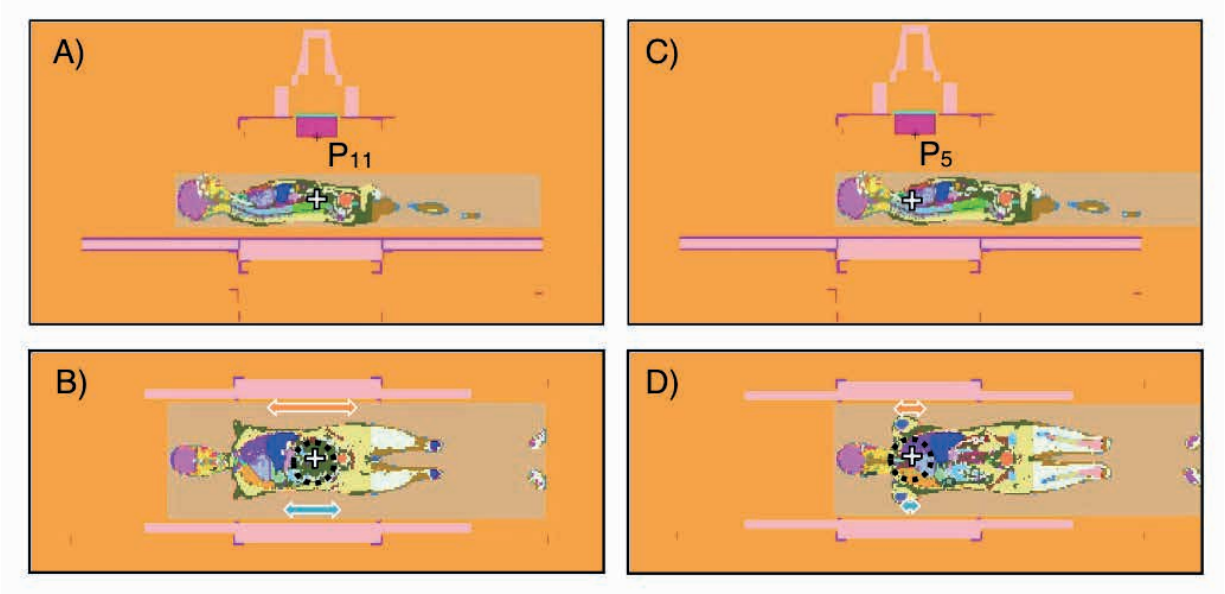

Figure 4: Reference points for monitoring uniformly distributed sources in soft tissues (A and B) and sources distributed in the lungs (C and D). The blue arrows indicate the area whose positioning errors on the longitudinal axis are less than 5% and the green arrows indicate the area with errors less than 10%. The dotted circles represent the projection of the detector on the body.

support this research project: ``*Fundação de Amparo à Pesquisa do Estado de Minas Gerais``* (FAPEMIG - Project APQ-03582-18), National Council for Scientific and Technological Development (CNPq) and Graduate Personnel Training Coordination (CAPES).

REFERENCES

ANSI, 1999. American National Standard: Specifications for the bottle manikin absorption phantom.

Bento, J., Barros, S., Teles, P., Neves, M., Gonçalves, I., Corisco, J., Vaz, P., 2012. Monte carlo simulation of the movement and detection efficiency of a whole-body counting system using a bomab phantom. Radiat Prot Dosimetry 148, 403–413. https://doi.org/10.1093/rpd/ncr201

Bhati, S., Patni, H.K., Ghare, V.P., Singh, I.S., Nadar, M.Y., 2012. Monte carlo calculations for efficiency calibration of a whole-body monitor using BOMAB phantoms of different sizes. Radiat Prot Dosimetry 148, 414–419. https://doi.org/10.1093/rpd/ncr203

Böke, A., 2014. Linear attenuation coefficients of tissues from 1keV to 150keV. Radiation Physics and Chemistry 102, 49–59. https://doi.org/10.1016/j.radphyschem.2014.04.006

Carr, D.J., Stevenson, T., Mahoney, P.F., 2018. The use of gelatine in wound ballistics research. Int J Legal Med. https://doi.org/10.1007/s00414-018-1831-7

ChemBK, n.d. Gelatin - Physico-Chemical Properties [WWW Document]. URL https://www.chembk.com/en/chem/Gelatin

Dantas, B.M., 1998. Bases para a Calibração de Contadores de Corpo Inteiro Utilizando Simuladores Físicos Antropomórficos. Universidade do Estado do Rio de Janeiro, Rio de Janeiro.

Dantas, B.M., Dantas, A.L.A., Acar, M.E.D., Cardoso, J.C.S., Julião, L.M.Q.C., Lima, M.F., Taddei, M.H.T., Arine, D.R., Alonso, T., Ramos, M.A.P., Fajgelj, A., 2011. Accreditation and training on internal dosimetry in a laboratory network in Brazil: An increasing demand. Radiat Prot Dosimetry 144, 124–129. https://doi.org/10.1093/rpd/ncq412

Ellis-Akovali, Y.A., 1987. A = 226 NUCLEAR DATA SHEETS A = 226. Oak Ridge.

Ferreira, C.V.G., Piedade, J.S., Prado, M.R.D., Benavente, J., Mendes, B.M., Paixão, L., Fonseca, T.C.F., 2023. Monte Carlo calculation of whole body counter efficiency factors for different computational phantoms. Applied Radiation and Isotopes 194. https://doi.org/10.1016/j.apradiso.2023.110685

Fonseca, T.C.F., Bogaerts, R., Hunt, J., Vanhavere, F., 2014a. A methodology to develop computational phantoms with adjustable posture for WBC calibration. Phys Med Biol 59, 6811–6825. https://doi.org/10.1088/0031-9155/59/22/6811

Fonseca, T.C.F., Bogaerts, R., Lebacq, A.L., Ribeiro, R.M., Vanhavere, F., 2014b. MaMP and FeMP: Computational mesh phantoms applied for studying the variation of WBC efficiency using a NaI(Tl) detector. Journal of Radiological Protection 34, 529–543. https://doi.org/10.1088/0952-4746/34/3/529

Hamad, K., Kaseem, M., Yang, H.W., Deri, F., Ko, Y.G., 2015. Properties and medical applications of polylactic acid: A review. Express Polym Lett 9, 435–455. https://doi.org/10.3144/expresspolymlett.2015.42

ICRP, 2009. Adult Reference Computational Phantoms. Ann ICRP 39, 21–45. https://doi.org/10.1016/j.icrp.2009.07.004

ICRU, I.C. on R.U. and Measurements., 1992. Phantoms and computational models in therapy, diagnosis, and protection. International Commission on Radiation Units and Measurements.

ICRU, I.C. on R.U. and Measurements., 1989. Tissue substitutes in radiation dosimetry and measurement. International Commission on Radiation Units and Measurements.

Jayachandran, C.A., 1971. Calculated effective atomic number and Kerma values for tissue-equivalent and dosimetry materials, Physics in Medicine & Biology A Jayachandran.

Jusufbegović, M., Pandžić, A., Šehić, A., Jašić, R., Julardžija, F., Vegar-Zubović, S., Beganović, A., 2022. Computed tomography tissue equivalence of 3D printing materials. Radiography 28, 788–792. https://doi.org/10.1016/j.radi.2022.02.008

Kerkhoff, W., Visser, M., Mattijssen, E., Hermsen, R., Alberink, I., 2022. A combined cowhide/gelatine soft tissue simulant for ballistic studies. Forensic Sci Int. https://doi.org/10.1016/j.forsciint.2022.111392

Kovtun, A.N., Firsanov, V.B., Forminykh, V.I., Isaakyan, G.A., 2000. Metrological parameters of the unified calibration whole-body phantom with gamma-emmiting radionuclides. Radiat Prot Dosimetry 89, 239–242.

Kramer, R., Khoury, H.J., Vieira, J.W., Loureiro, E.C.M., Lima, V.J.M., Lima, F.R.A., Hoff, G., 2004. All about FAX: A Female Adult voXel phantom for Monte Carlo calculation in radiation protection dosimetry. Phys Med Biol 49, 5203–5216. https://doi.org/10.1088/0031-9155/49/23/001

Kramer, R., Vieira, J.W., Khoury, H.J., Lima, F.R.A., Fuelle, D., 2003. All about MAX: a male adult voxel phantom for Monte Carlo calculations in radiation protection dosimetry, MEDICINE AND BIOLOGY Phys. Med. Biol.

Lebacq, A.L., Bruggeman, M., Vanhavere, F., 2011. Efficiency calibration of a whole-body-counting measurement setup using a modular physical phantom. Radiat Prot Dosimetry 144, 411–414. https://doi.org/10.1093/rpd/ncq575

MCNP® User's Manual Code Version 6.2, 2017.. Los Alamos National Security, LLC. LA-UR-17-29981.

NIST, N.I. of S. and T., n.d. NIST XCOM: Photon Cross Sections Database [WWW Document].

Özdemir, M., Özdemir, G., Eroğul, O., 2019. Investigating ballistic gelatin based phantom properties for ultrasound training, in: IFMBE Proceedings. Springer Verlag, pp. 789–793. https://doi.org/10.1007/978-981-10-9035-6_145

Pacheco, D., 2023. Modelagem, validação e teste da blindagem do contador de corpo inteiro e da sala de monitoração do LDI, utilizando código de Monte Carlo (Dissertation). Centro de Desenvolvimento da Tecnologia Nuclear, Belo Horizonte.

Paiva, F.G., Mendes, B.M., Da Silva, T.A., Lacerda, M.A.S., Pinto, J.R., Prates, S., Filho, N.N.A., Dantas, A.L.A., Dantas, B.M., Fonseca, T.C.F., 2017. Calibration of the LDI/CDTN Whole Body Counter using three physical phantoms. Brazilian Journal of Radiation Sciences.

Paiva, F.G., Oliveira, A.H. de, Mendes, B.M., Pinto, J.R., Filho, N. do N.A., Dantas, B.M., Dantas, A.L.A., Silva, T.A. da, Lacerda, M.A. de S., Fonseca, T.C.F., 2016. Improvement of the WBC calibration of the Internal Dosimetry Laboratory of the CDTN/CNEN using the physical phantom BOMAB and MCNPX code. Appl Radiat Isot 117, 123–127. https://doi.org/10.1016/j.apradiso.2015.12.059

Paquet, F., Etherington, G., Bailey, M.R., Leggett, R.W., Lipsztein, J., Bolch, W., Eckerman, K.F., Harrison, J.D., 2015. Annals of the ICRP Occupational Intakes of Radionuclides: Part 1.

Paquet, F., Leggett, R.W., Blanchardon, E., Bailey, M.R., Gregoratto, D., Smith, T., Ratia, G., Davesne, E., Berkovski, V., Harrison, J.D., 2022. Occupational Intakes of Radionuclides: Part 5. Ann ICRP 51, 11–415. https://doi.org/10.1177/01466453211028755

Park, M.S., Kim, H.S., Yoo, J., Kim, C.H., Jang, W. Il, Park, S., 2021. Virtual calibration of whole-body counters to consider the size dependency of counting efficiency using Monte Carlo simulations. Nuclear Engineering and Technology 53, 4122–4129. https://doi.org/10.1016/j.net.2021.06.026

Park, M.S., Yoo, J., Kim, M., Jang, W. Il, Park, S., 2023. Determination of counting efficiency considering the biodistribution of 131I activity in the whole-body counting measurement. Nuclear Engineering and Technology 55, 295–303. https://doi.org/10.1016/j.net.2022.09.013

PNNL, P.N.N.L., 2021. Data Mining Analysis and Modeling Cell Compendium of Material Composition Data for Radiation Transport Modeling.

Savi, M., Villani, D., Andrade, M.A.B., Rodrigues, O., Potiens, M.P.A., 2021. Study on attenuation of 3D printing commercial filaments on standard X-ray beams for dosimetry and tissue equivalence. Radiation Physics and Chemistry 182. https://doi.org/10.1016/j.radphyschem.2021.109365

Schläger, M., 2011. Comparison of various anthropomorphic phantom types for in vivo measurements by means of Monte Carlo simulations. Radiat Prot Dosimetry 144, 384–388. https://doi.org/10.1093/rpd/ncq320

Takahashi, M., Kinase, S., Kramer, R., 2011. Evaluation of counting efficiencies of a whole-body counter using Monte Carlo simulation with voxel phantoms. Radiat Prot Dosimetry 144, 407–410. https://doi.org/10.1093/rpd/ncq417

Tekin, H.O., Singh, V.P., Altunsoy, E.E., Manici, T., Sayyed, M.I., 2017. Mass attenuation coefficients of human body Organs using MCNPX Monte Carlo Code. Iranian Journal of Medical Physics 14, 229–240. https://doi.org/10.22038/ijmp.2017.23478.1230

Toth, K.S., 1977. Nuclear Data Sheets for A = 222*, Nuclear Data Sheets. Oak Ridge.

Vital, K.D., Mendes, B.M., de Sousa Lacerda, M.A., da Silva, T.A., Ferreira Fonseca, T.C., 2019. Development of a physical head phantom using of a solid brain equivalent tissue for the calibration of the 18F-FDG internal monitoring system. Radiation Physics and Chemistry 155, 56–61. https://doi.org/10.1016/j.radphyschem.2018.08.037

Zerby, C.D., Meyer, A., Murray, R.B., 1961. Intrinsic line broadening in NaI(Tl) gamma-ray spectrometers. Nuclear Instruments and Methods 12, 115–123. https://doi.org/https://doi.org/10.1016/0029-554X(61)90119-7

Zhang, B., Mille, M., Xu, X.G., 2008. An analysis of dependency of counting efficiency on worker anatomy for in vivo measurements: Whole-body counting. Phys Med Biol 53, 3463–3475. https://doi.org/10.1088/0031-9155/53/13/004